Pulmonary arterial elasticity in awake dogs

BRYDON J. B. GRANT, JOHN M. CANTY, JR., G. SRINIVASAN, AND ALAN S. BRODY
Departments of Medicine and Pediatric Radiology, State University of New York at Buffalo, Buffalo, New York 14215

GRANT, BRYDON J. B., JOHN M. CANTY, JR., G. SRINIVASAN, AND ALAN S. BRODY. *Pulmonary arterial elasticity in awake dogs.* J. Appl. Physiol. 75(2): 840–848, 1993.—We measured the relationship between pulmonary arterial pressure (Ppa), diameter (D), and length of a segment of the main pulmonary artery (MPA) in chronically instrumented conscious dogs breathing spontaneously (CCC). There were no physiologically significant changes in Ppa or D in the CCC dogs postoperatively, and the cross-sectional MPA shape measured by fast computed tomography was nearly circular. These results suggest that the MPA was not distorted by chronic instrumentation. We compared measurements made in the CCC dogs with previous measurements in acutely instrumented anesthetized dogs with open chests (AAO). The elasticity of MPA in the CCC animals was frequency dependent between 1 and 14 Hz and was similar to that in the AAO dogs. Oscillations of D preceded Ppa at cardiac frequencies in the AAO animals, but the D and Ppa oscillations were in phase in the CCC animals. The oscillations of length relative to D were significantly less in the CCC than in the AAO dogs. We conclude that, with limitations, the hemodynamic properties of the MPA can be measured in the CCC subjects. We suggest that the discrepancies between the AAO and CCC dogs can be attributed to differences in extrinsic loading of the MPA.

characteristic impedance; vascular compliance; sonomicrometry

HEMODYNAMIC STUDIES of the pulmonary circulation in conscious dogs have been directed primarily to measuring pulmonary vascular resistance, which represents the opposition to mean blood flow through the lungs. Resistance is an incomplete description of ventricular afterload because it neglects the opposition to the pulsatile components of blood flow (17). In fact, between 33 and 48% of hydraulic power in the main pulmonary artery (MPA) is contained in the oscillatory component (19).

Anesthesia can have marked effects on the physiological responses. For example, pentobarbital sodium alters the pulmonary vascular response to autonomic antagonists (20). Therefore, the need arises to study conscious animals. Previous methods for studying the pulsatile properties of the pulmonary circulation in conscious dogs have measured pressure and flow in the MPA (7). These measurements are used to calculate characteristic impedance from the input impedance spectrum. Flow was measured with a perivascular electromagnetic flow probe placed on the MPA.

The several drawbacks to this approach are due to limitations in the measurement of blood flow. First, we have found that perivascular flow probes may distort the impedance spectrum in acute preparations (12). Although the placement of flow probes in chronically instrumented animals does not require constriction of the MPA, extensive dissection around the MPA is needed for their placement. As a result, the neural supply of the proximal pulmonary arteries may be impaired and the healing process may distort the anatomy and elasticity of the MPA. Second, the measurement of characteristic impedance does not provide any information about the mechanisms that result in changes in this variable. Changes in characteristic impedance could result from alterations in the dimensions or elasticity of the MPA or both.

To overcome these difficulties, we measured the pulmonary arterial pressure (Ppa) and diameter (D) of the MPA in conscious dogs. D was measured by sonomicrometry. Unlike flow probes, placement of ultrasonic crystals does not require complete dissection around the MPA. Furthermore, the alterations in the dimensions and elasticity of the MPA with this approach are measured directly without having to surmise the physiological response from changes in characteristic impedance. Previously, we made measurements of Ppa, D, and segment length (L) of the MPA in acutely instrumented dogs (11). This report describes three series of experiments in chronically instrumented dogs.

In the first series of experiments, Ppa and D were measured between 3 and 64 postoperative days to determine the temporal changes that may occur after surgery. In a second series of experiments, the three-dimensional shape of the MPA was obtained from fast computed tomographic (CT) images. A third series of experiments was conducted to measure the Peterson's elastic modulus of the MPA from the oscillatory changes in Ppa and D of the MPA in conscious dogs over a range of frequencies. The similarity of the changes in the MPA dimensions in both its transverse and longitudinal axes (orthotropic behavior) was assessed from the relative amplitudes of the D and L oscillations. These measurements made in chronically instrumented conscious dogs with closed chests (CCC) were compared with previous measurements made in acutely instrumented anesthetized dogs with open chests (AAO) (11).

Both Peterson's elastic modulus for D (Ep_D) and the L-D relationship (LDR) depend not only on their mechanical properties but also on the loading conditions to which the MPA is subjected. We hypothesized that there would be differences in the elasticities of the MPA measured between the CCC and AAO animals because the

extrinsic loading conditions of the MPA differ markedly. In the CCC dogs, the MPA is more constrained by surrounding tissue within the closed chest.

METHODS

Preparation of chronically instrumented animals. Details of the experimental preparation for the first series of experiments have been described before (5). In brief, anesthesia was induced in mongrel dogs ($n = 11$) with an intravenous injection of sodium thiamylal (20 mg/kg). The dogs were then ventilated with a mixture of ~2% halothane and 70% nitrous oxide in oxygen. Succinylcholine (1 mg/kg) was used for muscular relaxation while the dogs were in the surgical plane of anesthesia. A left thoracotomy through the fifth intercostal space was performed with sterile surgical techniques. Two ultrasonic crystals on Dacron patches were sutured to the adventitia of the MPA. The crystals were aligned in a plane perpendicular to the direction of flow. A short 22-gauge Teflon angiocath was introduced gently into the pulmonary artery close to the site of the pair of diameter crystals. Additional Tygon catheters were placed in the descending thoracic aorta and the left atrium. These animals were used for other experiments (5) and were instrumented with equipment that was not required for the present study. This additional instrumentation included pacing wires, ultrasonic crystals in the left ventricle, a hydraulic occluder around the left circumflex coronary artery, and a Konigsberg micromanometer in the left ventricle. The chest was closed, and the pneumothorax was evacuated.

The dogs were treated with intramuscular procaine penicillin (300,000 U) and streptomycin (0.3 g) for 5 days. Intramuscular meperidine (50 mg) was given for analgesia during the first three postoperative days and was extended if required. The catheters were flushed every other day with saline and then filled with heparin (1,000 U/ml for atrium catheters, 10,000 U/ml for aorta and pulmonary artery catheters). The animals were brought to the laboratory as early as the third postoperative day for measurements to be made.

Dogs used in the second ($n = 5$) and third ($n = 6$) series of experiments were prepared similarly but with some changes in the chronic instrumentation. All cardiac instrumentation was omitted except for a left atrium catheter. Hydraulic occluders (Hazen-Everett, Teaneck, NJ, and Jones, Silver Spring, MD) were placed around the left main pulmonary artery and the inferior vena cava. In addition, ultrasonic crystals mounted on polystyrene attached to Dacron patches were sewn to the adventitia of the MPA to measure L.

Procedures for experiments in the conscious state. For the experiments that were conducted in the conscious state, the pulmonary artery catheters were attached to Statham P23 ID pressure transducers. The experiments were conducted with the animal in the right lateral decubitus or prone position. Zero pressure was assigned the level of the estimated position of the MPA. The ultrasonic crystals were attached to a sonomicrometer (model 120, Triton Technology, San Diego, CA) to measure D and L. The dogs were sedated with 1–3 ml of Innovar (droperidol 20 mg/ml and fentanyl 0.4 mg/ml, Pitman-Moore) only in the first series of experiments. Both Ppa and aortic pressure were displayed on an 8-channel Gould chart recorder. Data were digitized at 200 Hz/channel in the first series of experiments and at 250 Hz/channel in the third series. Circumferential extensibility (CE) of the MPA was calculated as the difference between the maximum and minimum values of D during a cardiac cycle expressed as a percentage of the mean and divided by the pulse pressure (23).

Experimental preparation for CT. Fast CT was performed in five additional mongrel dogs. Technically satisfactory images were obtained from two dogs (body wt 21.3–26.4 kg). The dogs were chronically instrumented as described above except that the crystals to measure L were omitted in one of the dogs to avoid artifacts in the CT images. The dogs were premedicated with 1–3 ml of Innovar through the left atrium catheter. In one dog, anesthesia was induced with 10 mg/kg of thiamylal followed by intravenous infusion at 11 $mg \cdot kg^{-1} \cdot h^{-1}$. The other dog was anesthetized with 25 mg/kg of pentobarbital sodium. In both dogs, intravenous pancuronium bromide (0.1 mg/kg) was used for muscular paralysis while the dog was in the surgical plane of anesthesia. The dogs were intubated and ventilated with a volume cycled pump (model 681, Harvard Apparatus, Natick, MA). The pump was used at a respiratory rate of 12–15/min with a tidal volume of 12 ml/kg. Supplemental oxygen (~50%) was given to avoid increases in Ppa during the scanning period of ~20 s while the ventilator was turned off to avoid respiratory movement.

Procedures for fast CT. The C-100 ultrafast CT scanner (Imatron, South San Francisco, CA) was used in the volume mode (24). In brief, the anesthetized dogs were placed in the gantry in the right lateral position. Each tomographic slice was 3 mm thick and was obtained in 100 ms. The resolution of each voxel was 0.7 × 0.7 × 3-mm slice thickness. The scanner was gated to the QRS complex of the electrocardiogram. Images were obtained during diastole at ~75% of the R-R′ interval. Multiple contiguous images were obtained in the region of the MPA with ventilation suspended at end expiration.

The images were analyzed with commercially available three-dimensional reconstruction software (ISG Allegro version 4.0, ISG Technologies, Mississauga, Ontario, Canada). The three-dimensional reconstructions were printed on 11 × 11-in. photographic paper with Kodak XL 7700 apparatus. Each cross-sectional image was outlined by at least 80 points with a Hitachi digitizing pad (resolution 0.0127 cm).

Frequency analysis. In the third series of experiments in unsedated awake dogs, the electrical signals of Ppa, D, and L were converted to digital form (DT2811, Data Translation, Marlborough, MA). The signals were displayed on the monitor of an IBM AT compatible computer (Dataq, Akron, OH). Recordings were made for 1 min at a sampling rate of 250 Hz/channel and were stored on disk for analysis. Spectral analysis was performed by the Blackman-Tukey method (3, 18). Details of the method are provided in the APPENDIX. The following equations were used to calculate the ratio of the amplitudes of the Ppa and D oscillations (R), its phase relation (ϕ), and the coherence (γ)

$$R_{1,2}(f) = \sqrt{\Phi_1(f)/\Phi_2(f)} \quad (1)$$

$$\phi_{1,2}(f) = \arctan[F_{1,2}(f)/E_{1,2}(f)] \quad (2)$$

$$\gamma^2_{1,2}(f) = [E_{1,2}(f)^2 + F_{1,2}(f)^2]/[\Phi_1(f) \cdot \Phi_2(f)] \quad (3)$$

where subscripts 1 and 2 refer to Ppa and D, respectively; Φ is the signal power at frequency f; and E and F are the cospectral (in phase) and quadrature (90° out of phase) powers of the cross spectrum power ($\Phi_{1,2}$), respectively. Therefore $\Phi_{1,2} = (E_{1,2} - jF_{1,2})$ where j is the square root of -1. $\gamma^2_{1,2}$ is the coherence function. The coherence provides a measure of linearity and is similar to the coefficient of determination (the square of Pearson's correlation coefficient). Ep_D was calculated from (11)

$$Ep_D(f) = R_{1,2}(f)D \quad (4)$$

Similar expressions were derived to assess the relationship between the oscillations of D and L. The magnitudes of these fluctuations of D and L were normalized for the mean D and L

$$LDR(f) = R_{3,2}(f)D/L \quad (5)$$

Subscripts 3 and 2 refer to the L and D oscillations, respectively. Therefore, LDR would be expected to be unity if the MPA were orthotropic such that elastic properties would be the same in both its transverse and longitudinal axes.

The results were corrected for the frequency response of the pressure transducer-catheter system. The natural frequency of the pressure system was 32 Hz, and the damping ratio was 0.0055 as measured by a pop test (8). The characteristics of the sonomicrometry filters were obtained from the manufacturer and were verified electrically in our instrument.

Statistical analysis. Analysis of variance for repeated-measures experimental design was used to assess the postoperative changes in Ppa, D, and CE. To analyze the spectra of Ep_D and LDR, we used maximum likelihood nonparametric regression. This approach was necessary because the accuracy of the estimate of $R_{1,2}$ varied with frequency. The details and the derivation of the weighting factors that were used are provided in the APPENDIX. At frequencies where $\gamma^2_{1,2}(f)$ is close to unity, the weighting factors become very large. As a result, the data at that frequency are emphasized compared with those at other frequencies where $\gamma^2_{1,2}(f)$ is small. The generalized additive models used for this purpose extend the more commonly used generalized linear models by cubic splines. This approach enables nonlinear relationships to be identified without presupposing any particular mathe-

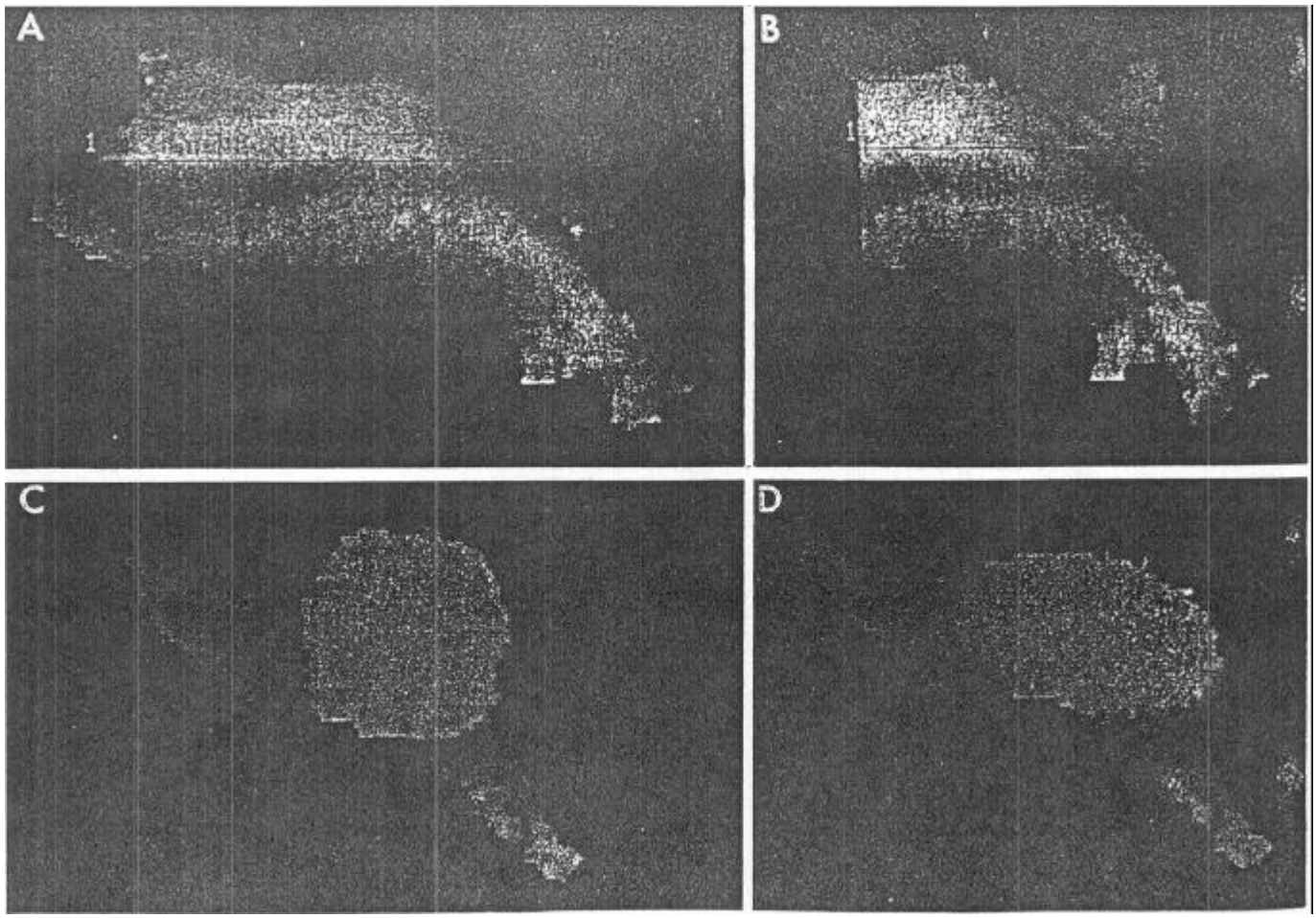

FIG. 1. Cross sections showing shape of main pulmonary artery. *A*: 3-dimensional reconstruction of main pulmonary artery of 1 dog, from pulmonary valve on *left* to bifurcation on *right*. *B*: same vessel transected at point close to sonomicrometer diameter crystals. *C*: same image rotated to expose cross section of almost circular shape of main pulmonary artery. *D*: elliptical cross section of same vessel immediately proximal to bifurcation.

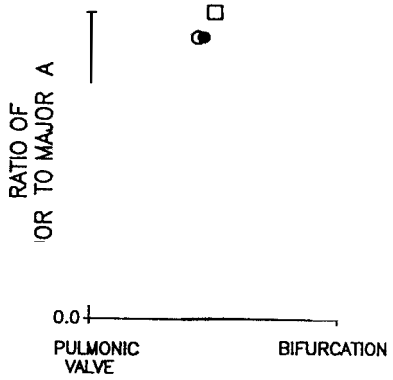

FIG. 2. Ratio of minor to major axes of main pulmonary artery plotted against approximate distance between pulmonary valve and bifurcation. Measurements are from 2 dogs (circles and square, respectively). Closed circles, measurements made during inflation of hydraulic occluder around inferior vena cava.

matical form. The order of the model was determined by minimizing the generalized cross-validation criterion, which is similar to the Akaike information criterion (14).

The perimeters of the cross section of the MPA were fitted to equations describing a circle and an ellipse. A least-squares approach was used to estimate the ratio of minor to major axes. Details of these procedures are described in the APPENDIX. An F test was used to determine if the data are more closely described by a circle (3 parameters) or an ellipse (5 parameters). In all instances, statistical significance was accepted at the 5% level and data are expressed as means ± SE.

RESULTS

Series 1: temporal changes in MPA. In our first series of experiments, dogs were studied from 2 to 42 days after surgery. Repeated measurements were made between postoperative *weeks 1* and *2* (n = 5 dogs) and beyond *week 2* (n = 6 dogs). These data were used to determine the temporal changes in mean Ppa, D, and CE. Between *weeks 1* and *2*, mean Ppa did not change significantly (24.2 ± 1.6 and 23.2 ± 2.2 cmH_2O, respectively). There was a small but statistically significant increase in D in each of the dogs (2.35 ± 0.12 to 2.40 ± 0.12 cm, respectively; $P < 0.01$) but no significant change in CE (0.385 ± 0.056 and 0.45 ± 0.044%/cmH_2O, respectively). After *week 2*, there were no significant changes in mean Ppa (21.2 ± 1.6 to 20.3 ± 2.3 cmH_2O, respectively), D (2.28 ± 0.11 and 2.34 ± 0.12 cm, respectively), or CE (0.572 ± 0.046 and 0.569 ± 0.064%/cmH_2O, respectively).

Series 2: shape of MPA. Figure 1 shows four three-dimensional images that were reconstructed from the fast CT data. Figure 1*A* shows a left lateral view of the MPA from the pulmonary valve (*left*) to the left and right pulmonary arteries (*right*). Figure 1*B* shows the same vessel transected close to the level of the diameter crystals. Figure 1*C* shows the same image rotated to expose the cross-sectional shape of the MPA, which is almost circular. Further sections through the MPA were similar in appearance except close to the bifurcation, where the MPA assumed an elliptical form (Fig. 1*D*).

Figure 2 plots the ratio of minor to major radii of the MPA against the proportional distance between the pulmonary valve and the bifurcation. The shape was maintained even when Ppa was decreased by full inflation of the hydraulic occluder around the inferior vena cava. This maneuver reduced the Ppa from 30/14 to 18/9 cmH_2O (systolic/diastolic).

Series 3: spectral analysis of MPA elasticity. Figure 3 shows a recording of Ppa, D, and L from a conscious dog in our second series of experiments. There are several differences compared with recordings from the AAO dog (11). First, a fluid-filled catheter was used to measure Ppa. The oscillations of ~32 Hz are related to the natural frequency of the catheter system that is absent from recordings in the acute preparation. A micromanometer-tipped catheter that has a natural frequency of 2,000 Hz was used in the acute preparation. Second, slow oscillations due to the respiratory cycle are less apparent in the conscious dog.

Figure 4 shows the mean Ep_D as a function of frequency in the CCC dogs (*top*). The corresponding values for phase angle and coherence function are shown in the *middle* and *bottom* panels, respectively. The *left* panels show results with narrow bandwidth at low frequencies (0–2 Hz). Ep_D varied significantly with frequency ($P <$ 0.001). Most of this variation occurred at <1.4 Hz, where the coherence function fell to low values (<0.7), indicating that the data are less reliable measures of the elastic properties of the pulmonary arterial wall at those frequencies. Above 1.4 Hz, there was little variation in Ep_D with frequency and the phase angle was close to zero for

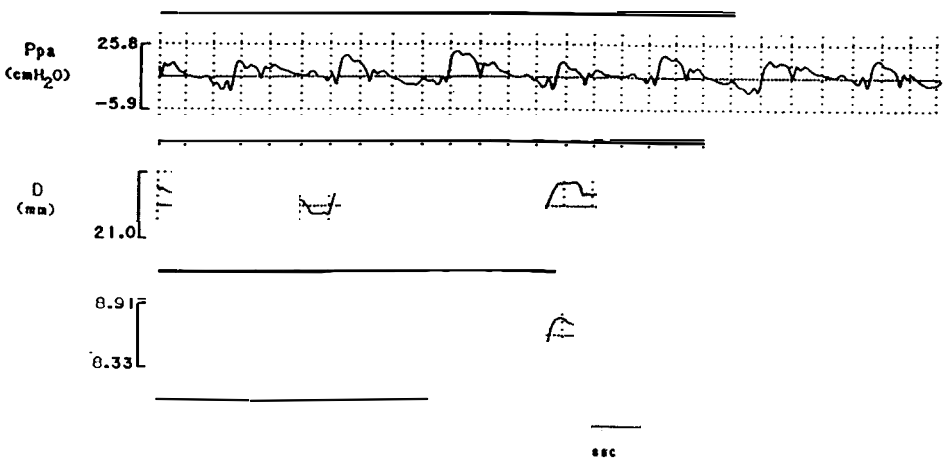

FIG. 3. Actual recording of pulmonary arterial pressure (Ppa), diameter (D), and length of segment (L) of main pulmonary artery in 1 conscious dog.

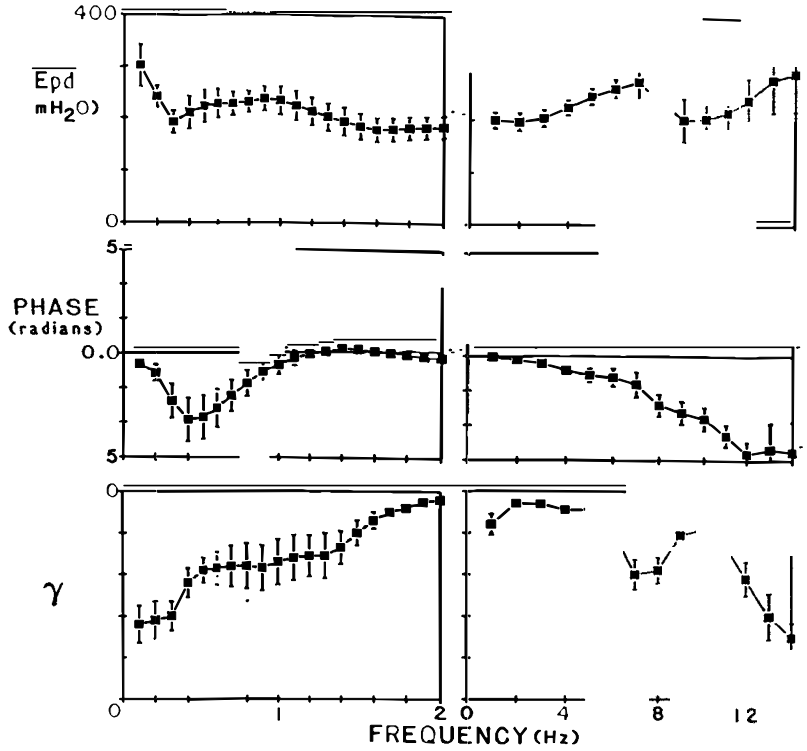

FIG. 4. Pressure strain modulus for D (Ep_D) measured in 6 conscious dogs. Each panel shows spectra averaged for dogs plotted against frequency. Bars, ±SE. *Left*: frequencies up to 2 Hz with narrow bandwidth (0.01 Hz). *Right*: frequencies up to 14 Hz with broad bandwidth (1 Hz). *Top*: modulus of Ep_D. *Middle*: phase relationship of Ep_D. Positive angles indicate that Ppa oscillations lead D oscillations. *Bottom*: coherence function of Ppa-D relationship (γ^2).

frequencies >1 Hz. The *right* panels show the results at high frequencies (0–14 Hz). There was a significant trend for Ep_D to increase with frequency ($P < 0.01$), and the phase angle was close to zero for frequencies <6 Hz. Above 6 Hz, the coherence function tended to fall.

Figure 5 shows the results for LDR. With the narrow bandwidth for frequencies up to 2 Hz (*left*), LDR did vary significantly with frequency ($P < 0.0001$). Similar to Ep_D, most of the variation of LDR with frequency occurred at <1.4 Hz, where the coherence function fell to low values. LDR was close to unity and the phase angle was close to zero for frequencies >0.8 Hz, but LDR became negative near 2 Hz. Negative phase angles indicate that D oscillations preceded L oscillations. With the broad bandwidth for frequencies up to 14 Hz (*right*), LDR did change significantly with frequency ($P < 0.0001$), but it remained fairly uniform and close to unity for frequencies up to 8 Hz. The phase angle was negative at <4 Hz but positive between 5 and 6 Hz. Above 6 Hz, the coherence function fell to low values.

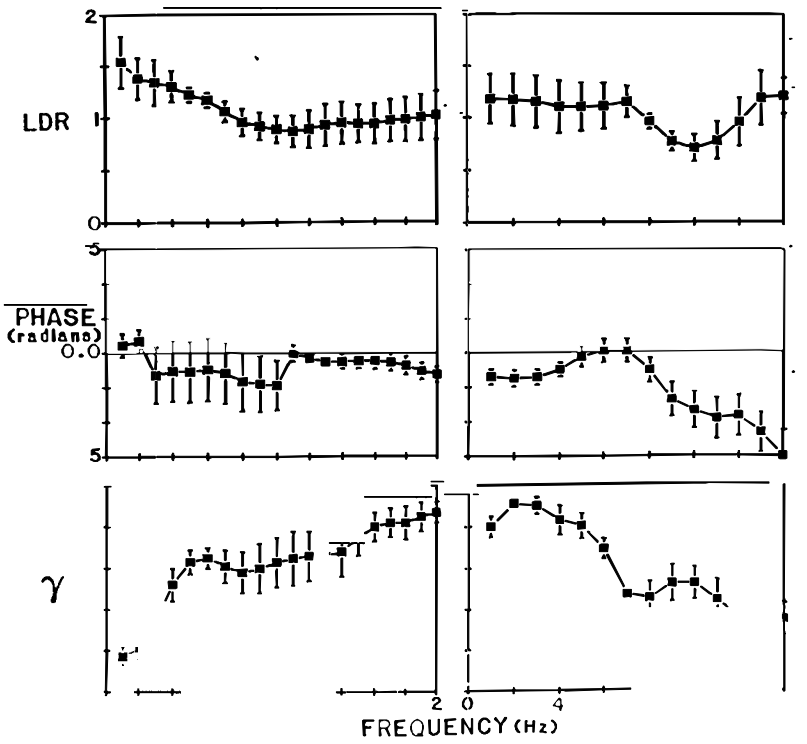

FIG. 5. L-D ratio (LDR) in same 6 chronically instrumented dogs. Each panel shows spectra averaged for dogs plotted against frequency. Bars, ±SE. *Top*: modulus of LDR. *Middle*: phase relationship of LDR. Positive angles indicate that L oscillations lead D oscillations. *Bottom*: coherence function of L-D relationship (γ^2).

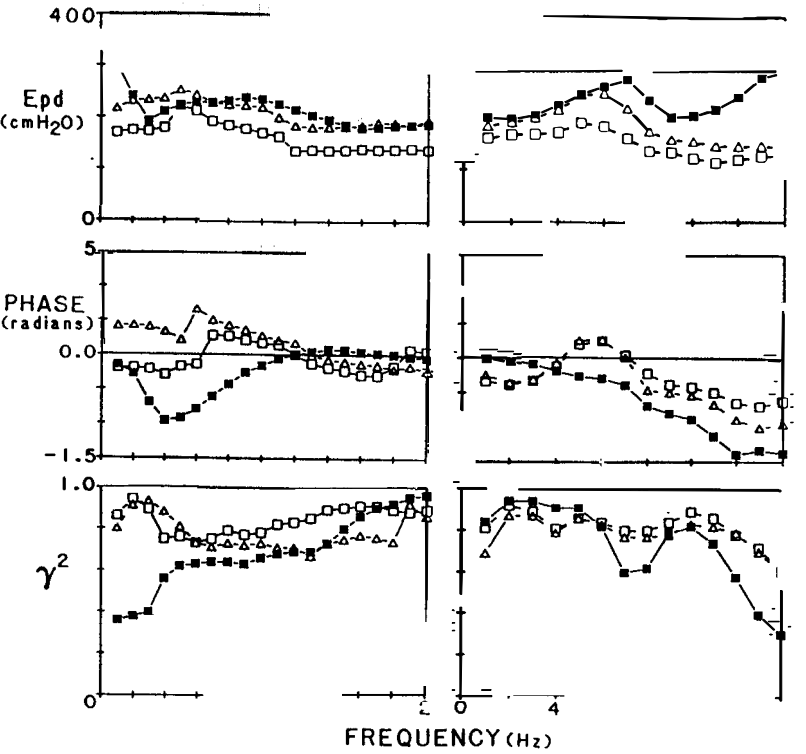

FIG. 6. Comparison of Ep_D measured in same 6 chronically instrumented dogs with measurements made in 6 acutely instrumented dogs. Each panel shows averaged spectra plotted against frequency. Solid squares, data from chronically instrumented dogs. For acutely instrumented dogs with open chest, open squares indicate 5 cmH_2O of positive end-expiratory pressure (PEEP) and open triangles indicate 10 cmH_2O of PEEP.

Figure 6 compares Ep_D in the CCC dogs to results obtained from a group of AAO dogs (11). With the narrow bandwidth for frequencies up to 2 Hz (*left*), Ep_D in the CCC subjects was similar to Ep_D at both 5 and 10 cmH_2O of positive end-expiratory pressure (PEEP) in the AAO animals. The coherence function remained high relative to that in the CCC dogs at <1.4 Hz and was greatest in the AAO dogs at ~0.2 Hz, which corresponds to the ventilator frequency.

Ep_D at the broad bandwidth for frequencies up to 14 Hz are shown in Fig. 6, *right*. Ep_D in the CCC animals is similar to Ep_D at 10 cmH_2O of PEEP but significantly different from measurements at a PEEP of 5 cmH_2O in the AAO dogs ($P < 0.005$). The pattern of frequency dependence of Ep_D was similar in both groups of dogs, with local maximal values occurring between 4 and 8 Hz. In contrast, the phase angle was negative at cardiac frequencies ~2 Hz in the AAO but not the CCC animals.

Figure 7 compares the measurement of LDR as a function of frequency in the CCC dogs with measurements

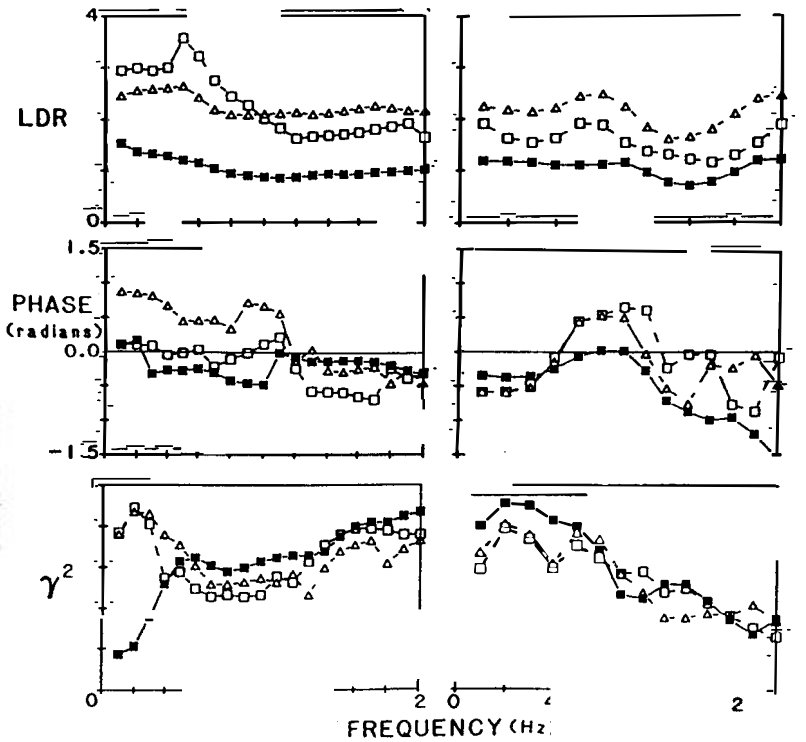

FIG. 7. LDR measured in same 6 chronically instrumented dogs compared with measurements made in same 6 acutely instrumented dogs. Each panel shows averaged spectra plotted against frequency. Solid squares, data for chronically instrumented dogs. For acutely instrumented dogs with open chest, open squares indicate 5 cmH_2O of PEEP and open triangles indicate 10 cmH_2O of PEEP.

obtained previously in the AAO subjects. With the narrow bandwidth for frequencies up to 2 Hz (*left*), LDR in the CCC animals was less than LDR in the AAO dogs at either level of PEEP ($P < 0.01$). LDR varied significantly with frequency (0–2 Hz) in a similar manner in both groups of dogs. The coherence function again showed the pattern seen in Fig. 5. The coherence function fell markedly in the CCC dogs at <0.5 Hz but rose in the AAO dogs that were ventilated at 0.2 Hz.

With the broad bandwidth for frequencies up to 14 Hz (Fig. 7, *right*), LDR in the CCC dogs was less than LDR in the AAO dogs at 10 cmH_2O of PEEP ($P < 0.001$) but not different from measurements made at 5 cmH_2O of PEEP. In both groups of dogs LDR varied significantly with frequency ($P < 0.005$), but frequency dependence of LDR was more marked in the AAO than in the CCC dogs. The corresponding phase angles and coherence functions were very similar in both groups of dogs.

DISCUSSION

Comparison of our results with previous studies. The advantage of a chronically instrumented preparation in studying the mechanical properties of the MPA is that it is free of the influence of anesthesia. Repeated measurements of drug effects are possible on different days on the same dog. This type of protocol requires the preparation to remain stable over the period of data collection. We found that 1 wk was sufficient to allow the preparation to stabilize in the first series of experiments. Nevertheless, we waited 2 wk postoperatively before experimentation in the second series of experiments, which were conducted without any sedation. We found that the dogs were more likely to lie still for the period of data collection after 2 wk of convalescence.

A potential problem with the chronically instrumented preparation is that scar tissue might distort the mechanical properties of the MPA. These results indicate that this problem does not occur. First, the measurements of CE are of similar magnitude to those obtained by others ($0.48 \pm 0.02\%/cmH_2O$) in acutely instrumented dogs (23). Second, the three-dimensional images of the MPA do not indicate any gross distortion or marked departure from an elliptical cross-sectional shape. Third, there were no marked differences of Ppa, D, or Ep_D during the postoperative period.

Cross-sectional shape of the MPA. Previous studies have suggested that the cross-sectional shape of the MPA is elliptical. This conclusion was based largely on models made from casts of the MPA (1, 16). The elliptical shape was apparent only with transmural distending pressures of <10 cmH_2O.

More recent in vivo studies support the view that the cross-sectional shape of the MPA is approximately circular. Johnson et al. (15) used two pairs of ultrasonic crystals to measure D in orthogonal planes. Their data indicate that the cross-sectional shape is almost circular: the median ratio of minor to major radii was 0.92 (10, 11). More recently, a similar result was obtained by two-dimensional intravascular ultrasonic imaging with an intravascular catheter that scans through 360° (21). The cross-sectional shape of the MPA in the anesthetized dog (Fig. 1 of Ref. 20) appeared circular. The investigators noted that it became elliptical at bifurcations.

Although our results are limited by the small number of animals used, they are in accord with these in vivo studies. Fast CT has the advantage of being able to generate three-dimensional images of anatomy in living animals. Although the alignment for the transected three-dimensional images was obtained by eye, the measurement of cross-sectional shape was objective. Even when Ppa was reduced by complete occlusion of the inferior vena cava, the MPA retained its cross-sectional shape.

Pulmonary arterial elasticity in the chronic preparation compared with in vitro data. Cox (6) measured the viscoelastic properties of canine pulmonary arteries in vitro. There was no marked frequency dependence. There was a small monotonic increase of ~6% in the dynamic elastic modulus between frequencies of 0.1 and 10 Hz. Our results show that Ep_D is clearly frequency dependent in both the CCC and AAO dogs over the range of 1–10 Hz. Therefore, this frequency dependence cannot be explained by any intrinsic behavior of the pulmonary arterial wall. The pattern of the variation in Ep_D with frequency is similar in both groups of dogs. Therefore, it is unlikely to be due to the extrinsic loading conditions of the MPA because these are markedly different between the two preparations. A more likely explanation is that the variation is due to cardiac motion.

Diastolic filling of the right ventricle may result in movement of the pulmonary valve along the long axis of the MPA. This motion would tend to shorten the MPA and increase D to maintain volume, all other factors being equal. During systole, ventricular contraction may tend to pull on the MPA and stretch its longitudinal axis and diminish its transverse dimensions. Therefore, it seems possible that cardiac motion could modify the elastic properties of the MPA by a direct effect. Further studies would be required to test this hypothesis.

Pulmonary arterial elasticity in chronic and acute preparations. In general, Ep_D in the CCC dogs was similar to that in the AAO dogs. CE was similar to that measured by others in AAO dogs (23). Nevertheless, there are two important differences that deserve further comment.

First, coherence fell markedly for frequencies <0.5 Hz in the CCC dogs, so there is less confidence in the data at those frequencies. The low coherence suggests that the oscillatory changes in Ppa and D are not linearly related. In the AAO dogs, the chest is open such that the extramural pressure is close to atmospheric pressure. Therefore, the measured Ppa approximates the transmural pressure. At respiratory frequencies, a high coherence is anticipated because D is dependent primarily on the transmural pressure. In the CCC dogs, however, the extramural pressure varied due to spontaneous breathing because the extramural pressure of the MPA is related to pleural pressure. Therefore, the measured intraluminal changes of Ppa in CCC dogs do not reflect the transmural changes of Ppa at respiratory frequencies. As a result, the coherence relationship will be impaired.

The second difference is the negative phase relationship between Ppa and D at the cardiac frequency seen in the AAO dogs (11). We have confirmed that observation in this report with spectral analysis rather than the

Fourier analysis that we used previously (11). The negative phase relationship did not occur in the CCC dogs. The negative phase relationship indicates that changes in D preceded changes in Ppa. We also observed that negative phase angles of Ep_D occurred at higher frequencies (>10 Hz). Because of the low coherence at higher frequencies, these negative phase angles may be related to nonlinearities in the Ppa-D relationship as demonstrated by Gow and Taylor (9). At cardiac frequencies the coherence was high; therefore, the negative phase relationships are unlikely to be attributed to nonlinearities.

Previously, we advanced two explanations for the negative phase relationships at cardiac frequencies. First, the negative phase angle may be related to cardiac motion. As indicated earlier, ventricular filling during diastole may result in forward motion of the pulmonary valve along the longitudinal axis of the MPA and result in an increase in D before the increase in Ppa. Second, Womersley's theory predicts that negative phase relationships can occur in a purely elastic tube (25). According to this theory, the increased D precedes Ppa due to the fact that more flow is entering the segment of the MPA than leaving it in early systole because flow is accelerating.

Although differences in cardiac motion between the CCC and AAO animals cannot be discounted, there is a clear difference in the external loading of the MPA. The different pattern in the CCC dogs is not surprising because the chest is closed and the wall of the MPA is loaded by surrounding tissue. Under these circumstances, the MPA cannot be considered a freely mobile elastic tube.

The most obvious difference in the results obtained with the CCC and AAO dogs was for LDR. In the dogs with closed chests, LDR is close to unity and is frequency independent. In the dogs with open chests, LDR is greater than unity. An LDR greater than unity indicates that the fractional changes in L are greater than the corresponding changes in D. This result suggests that the external loading of the MPA constrains the movement of the vessel more in its longitudinal axis than in its transverse axis. With the chest open, lung expansion may result in greater movement of the lung from the heart that would tend to elongate the MPA and would account for the larger differences in LDR between the CCC and AAO dogs at respiratory frequencies.

The hypothesis that cardiac motion contributes to the longitudinal motion of the great vessels is not new. Patel and Fry (22) compared the longitudinal extensibility to the CE. This ratio is analogous to our LDR at cardiac frequency. They indicated that the ratio is ~0.83 in the ascending aorta, whereas it is only 0.33 in the midthoracic descending aorta. The negative phase angles at cardiac frequencies indicate that changes in D preceded changes in L. This finding is compatible with the hypothesis that cardiac motion modulates the dimensions of the MPA.

In conclusion, the chronically instrumented preparation has both advantages and disadvantages over the acutely instrumented preparation. On the one hand, the need for anesthesia during data collection is avoided. In addition, the animals are studied in a situation that is close to normal operating conditions. On the other hand, there are limitations. The measurement of Ppa is intraluminal and does not represent the transmural pressure at respiratory frequencies. As a result, the measurement of Ep_D at frequencies less than cardiac frequency is a less reliable measure of elastic properties of the pulmonary arterial wall.

APPENDIX

Frequency Analysis

The data were sampled at 250 Hz/channel. Before spectral analysis, the data were decimated to produce a slower sampling frequency. The data were filtered before decimation with a digital filter to prevent aliasing (2).

To reduce the data record to a frequency of 50 Hz, the raw data at 250 Hz/channel were processed first through a digital filter with a half-power frequency of 15 Hz, a roll-off of 10 db/octave, and <3% power in the side lobes. This filtering was achieved by using techniques described by Hamming (13). The data were submitted to a 5-point and then a 9-point moving average. The roll-off of the filter was increased by doubling the output of the filter and subtracting it from the original tripled values. The moving averages were then repeated twice. Decimation was achieved by selecting every fifth data point. Spectral analysis was performed on the decimated data by the Blackman-Tukey method (4). A Hanning taper was applied to the correlation functions to avoid any discontinuity between the beginning and end of the data record. The maximum lag was <1% of the data record to produce a bandwidth of 1 Hz. The data were reanalyzed with a narrower bandwidth over a lower range of frequencies (0–2 Hz). The decimated data were then processed through a similar digital filtering process but with moving averages of 9 and 19 points. The half power of this filter was at 1.5 Hz with a roll-off of 12 db/octave. The decimation process was repeated by selecting every tenth data point to produce a sampling rate of 5 Hz. The maximum lag used was 8% of the data record, resulting in a bandwidth of 0.1 Hz.

The decimated data were analyzed by the Blackman-Tukey method (4). The same equations described in detail by Milnor (18) for the pressure-flow relationship were used to determine the Ppa-D and L-D relationships. The power and cross-power spectra of the corresponding variables were calculated from the autocorrelations and cross correlations.

Weighting Function

To calculate a weighting function for statistical analysis, the errors in Ep_D and LDR were assumed to be due to Ppa and L, respectively. This assumption is a reasonable approximation, at least for Ep_D. Ppa is subject to greater variation than D because of respiratory motion and the inferior frequency response of the fluid-filled catheter system compared with sonomicrometry. It has been shown that the noise power spectrum $[\Phi_n(f)]$ can be expressed as follows (see chapt. 6 of Ref. 2)

$$\Phi_n(f) = [1 - \gamma^2_{1,2}(f)]\Phi_1(f) \qquad (A1)$$

The variance (Var) of $R_{1,2}(f)$ can be approximated by

$$\mathrm{Var}[R_{1,2}(f)] = [\Phi_n(f)/\Phi_2(f)] \qquad (A2)$$

By substituting in *Eq. A2* for $\Phi_n(f)$ from *Eq. A1*

$$\mathrm{Var}[R_{1,2}(f)] = [1 - \gamma^2_{1,2}(f)]R^2_{1,2}(f) \qquad (A3)$$

Therefore, the weighting factor that was used was the inverse of $\mathrm{Var}[R_{1,2}(f)]$.

The weighting factor for a phase angle is the inverse of its

Fourier analysis that we used previously (11). The negative phase relationship did not occur in the CCC dogs. The negative phase relationship indicates that changes in D preceded changes in Ppa. We also observed that negative phase angles of Ep_D occurred at higher frequencies (>10 Hz). Because of the low coherence at higher frequencies, these negative phase angles may be related to nonlinearities in the Ppa-D relationship as demonstrated by Gow and Taylor (9). At cardiac frequencies the coherence was high; therefore, the negative phase relationships are unlikely to be attributed to nonlinearities.

Previously, we advanced two explanations for the negative phase relationships at cardiac frequencies. First, the negative phase angle may be related to cardiac motion. As indicated earlier, ventricular filling during diastole may result in forward motion of the pulmonary valve along the longitudinal axis of the MPA and result in an increase in D before the increase in Ppa. Second, Womersley's theory predicts that negative phase relationships can occur in a purely elastic tube (25). According to this theory, the increased D precedes Ppa due to the fact that more flow is entering the segment of the MPA than leaving it in early systole because flow is accelerating.

Although differences in cardiac motion between the CCC and AAO animals cannot be discounted, there is a clear difference in the external loading of the MPA. The different pattern in the CCC dogs is not surprising because the chest is closed and the wall of the MPA is loaded by surrounding tissue. Under these circumstances, the MPA cannot be considered a freely mobile elastic tube.

The most obvious difference in the results obtained with the CCC and AAO dogs was for LDR. In the dogs with closed chests, LDR is close to unity and is frequency independent. In the dogs with open chests, LDR is greater than unity. An LDR greater than unity indicates that the fractional changes in L are greater than the corresponding changes in D. This result suggests that the external loading of the MPA constrains the movement of the vessel more in its longitudinal axis than in its transverse axis. With the chest open, lung expansion may result in greater movement of the lung from the heart that would tend to elongate the MPA and would account for the larger differences in LDR between the CCC and AAO dogs at respiratory frequencies.

The hypothesis that cardiac motion contributes to the longitudinal motion of the great vessels is not new. Patel and Fry (22) compared the longitudinal extensibility to the CE. This ratio is analogous to our LDR at cardiac frequency. They indicated that the ratio is ~0.83 in the ascending aorta, whereas it is only 0.33 in the midthoracic descending aorta. The negative phase angles at cardiac frequencies indicate that changes in D preceded changes in L. This finding is compatible with the hypothesis that cardiac motion modulates the dimensions of the MPA.

In conclusion, the chronically instrumented preparation has both advantages and disadvantages over the acutely instrumented preparation. On the one hand, the need for anesthesia during data collection is avoided. In addition, the animals are studied in a situation that is close to normal operating conditions. On the other hand, there are limitations. The measurement of Ppa is intraluminal and does not represent the transmural pressure at respiratory frequencies. As a result, the measurement of Ep_D at frequencies less than cardiac frequency is a less reliable measure of elastic properties of the pulmonary arterial wall.

APPENDIX

Frequency Analysis

The data were sampled at 250 Hz/channel. Before spectral analysis, the data were decimated to produce a slower sampling frequency. The data were filtered before decimation with a digital filter to prevent aliasing (2).

To reduce the data record to a frequency of 50 Hz, the raw data at 250 Hz/channel were processed first through a digital filter with a half-power frequency of 15 Hz, a roll-off of 10 db/octave, and <3% power in the side lobes. This filtering was achieved by using techniques described by Hamming (13). The data were submitted to a 5-point and then a 9-point moving average. The roll-off of the filter was increased by doubling the output of the filter and subtracting it from the original tripled values. The moving averages were then repeated twice. Decimation was achieved by selecting every fifth data point. Spectral analysis was performed on the decimated data by the Blackman-Tukey method (4). A Hanning taper was applied to the correlation functions to avoid any discontinuity between the beginning and end of the data record. The maximum lag was <1% of the data record to produce a bandwidth of 1 Hz. The data were reanalyzed with a narrower bandwidth over a lower range of frequencies (0–2 Hz). The decimated data were then processed through a similar digital filtering process but with moving averages of 9 and 19 points. The half power of this filter was at 1.5 Hz with a roll-off of 12 db/octave. The decimation process was repeated by selecting every tenth data point to produce a sampling rate of 5 Hz. The maximum lag used was 8% of the data record, resulting in a bandwidth of 0.1 Hz.

The decimated data were analyzed by the Blackman-Tukey method (4). The same equations described in detail by Milnor (18) for the pressure-flow relationship were used to determine the Ppa-D and L-D relationships. The power and cross-power spectra of the corresponding variables were calculated from the autocorrelations and cross correlations.

Weighting Function

To calculate a weighting function for statistical analysis, the errors in Ep_D and LDR were assumed to be due to Ppa and L, respectively. This assumption is a reasonable approximation, at least for Ep_D. Ppa is subject to greater variation than D because of respiratory motion and the inferior frequency response of the fluid-filled catheter system compared with sonomicrometry. It has been shown that the noise power spectrum $[\Phi_n(f)]$ can be expressed as follows (see chapt. 6 of Ref. 2)

$$\Phi_n(f) = [1 - \gamma^2_{1,2}(f)]\Phi_1(f) \qquad (A1)$$

The variance (Var) of $R_{1,2}(f)$ can be approximated by

$$\mathrm{Var}[R_{1,2}(f)] = [\Phi_n(f)/\Phi_2(f)] \qquad (A2)$$

By substituting in *Eq. A2* for $\Phi_n(f)$ from *Eq. A1*

$$\mathrm{Var}[R_{1,2}(f)] = [1 - \gamma^2_{1,2}(f)]R^2_{1,2}(f) \qquad (A3)$$

Therefore, the weighting factor that was used was the inverse of $\mathrm{Var}[R_{1,2}(f)]$.

The weighting factor for a phase angle is the inverse of its

variance, which has been approximated by (see chapt. 9 of Ref. 2)

$$\mathrm{Var}[\phi_{1,2}(f)] = [1 - \gamma^2_{1,2}(f)]/\gamma^2_{1,2}(f) \qquad (A4)$$

Ellipticity of MPA Cross Section

To assess the ellipticity of the MPA cross section, we modified the standard equation for an ellipse. The coordinates of a point on the ellipse were expressed as (Msinθ, Mcosθ) instead of (x, y). M is $(x^2 + y^2)^{0.5}$, θ is arctan $[(y - k)/(x - h)]$, and (h, k) are the coordinates of the center of the ellipse. This modification was devised to introduce an additional term ϵ that describes the amount of rotation of the ellipse relative to the x and y axes. Thus, we used a least-squares criterion for the best fit to the perimeter of the digitized MPA image to

$$[\mathrm{Msin}(\theta + \epsilon) - h]^2/a^2 + [\mathrm{Mcos}(\theta + \epsilon) - k]^2/b^2 = 1 \qquad (A5)$$

where a and b are the major and minor radii, respectively. The criterion for a best fit was to minimize the residual sum of squares (RSS). The RSS is the sum of the square of the minimal distance of the digitized points (x_i, y_i) from the ellipse. The subscript i indicates one of the total number of points (N) on the two-dimensional surface that defines the perimeter of the cross section of the MPA image

$$\mathrm{RSS} = \sum^{i=N} [(x_i - x)^2 + (y_i - y)^2] \qquad (A6)$$

A Marquardt procedure (3) was used to optimize the five parameters (a, b, h, k, and ϵ). *Equation A5* was simplified to represent a circle

$$(x - h)^2 + (y - k)^2 = a^2 \qquad (A7)$$

For this equation, only three parameters need to be optimized: a, h, and k. The coordinates of a point on the circle are expressed as (x, y) instead of (Msin θ, Mcos θ) because the parameter ϵ is now superfluous. Parameter b is not required because it is always equal to parameter a.

We thank Amy Wurtenberger, Colleen Marx, the late Richard Kohlmeier, and Kathleen Harris of the State University of New York at Buffalo; Robert Kufchak, Karen Stanley, and Marianne Manns of Children's Hospital of Buffalo; and Joan Medley of ISG Technologies for their expert technical help; and Andy Wooster for programming assistance.

This study was supported by National Heart, Lung, and Blood Institute Grant R01-HL-41011.

Address for reprint requests: B. J. B. Grant, ECMC (Pulmonary Lab), 462 Grider St., Buffalo, NY 14215.

Received 5 October 1992; accepted in final form 17 March 1993.

REFERENCES

1. ATTINGER, E. O. Pressure transmission in pulmonary arteries related to frequency and geometry. *Circ. Res.* 12: 623–641, 1963.
2. BENDAT, J. S., AND A. G. PIERSOL. *Random Data Analysis and Procedures* (2nd ed.). New York: Wiley-Interscience, 1984.
3. BEVINGTON, P. R. *Data Reduction and Error Analysis for the Physical Sciences.* New York: McGraw-Hill, 1969, p. 204–246.
4. BLACKMAN, R. B., AND J. W. TUKEY. *The Measurement of Power Spectra.* New York: Dover, 1956, p. 31–49.
5. CANTY, J. M., JR. Coronary pressure-function and steady-state pressure-flow relations during autoregulation in the unanesthetized dog. *Circ. Res.* 63: 821–836, 1988.
6. COX, R. H. Viscoelastic properties of canine pulmonary arteries. *Am. J. Physiol.* 246 (*Heart Circ. Physiol.* 15): H90–H96, 1984.
7. ELKINS, R. C., AND W. R. MILNOR. Pulmonary vascular response to exercise in the dog. *Circ. Res.* 29: 591–599, 1971.
8. GABE, I. T. Pressure measurement in experimental physiology. In: *Cardiovascular Fluid Dynamics*, edited by D. H. Bergel. London: Academic, 1972, vol. 1, p. 11–49.
9. GOW, B. S., AND M. G. TAYLOR. Measurement of viscoelastic properties of arteries in the living dog. *Circ. Res.* 23: 111–122, 1968.
10. GRANT, B. J. B., AND J. M. CANTY, JR. Effect of cardiac output on pulmonary hemodynamics. *Respir. Physiol.* 76: 303–318, 1989.
11. GRANT, B. J. B., AND B. B. LIEBER. Compliance of the main pulmonary artery during the ventilatory cycle. *J. Appl. Physiol.* 72: 535–542, 1992.
12. GRANT, B. J. B., L. J. PARADOWSKI, AND J. M. FITZPATRICK. Effect of perivascular electromagnetic flow probes on pulmonary hemodynamics. *J. Appl. Physiol.* 65: 1885–1890, 1988.
13. HAMMING, R. W. *Digital Filters* (2nd ed.). Englewood Cliffs, NJ: Prentice-Hall, 1983.
14. HASTIE, T. J., AND R. J. TIBSHIRANI. *Generalized Additive Models.* New York: Chapman & Hall, 1990, p. 136–173.
15. JOHNSON, T. A., G. W. HENRY, C. L. LUCAS, B. A. KEAGY, M. E. LORES, H. S. HSIO, J. I. FERREIRO, AND B. R. WILCOX. Two-dimensional in vivo pressure/diameter relationships in the canine main pulmonary artery. *Cardiovasc. Res.* 19: 442–448, 1985.
16. MELBIN, J., AND A. NOORDERGRAAF. Elastic deformation in orthotropic vessels. *Circ. Res.* 28: 680–692, 1971.
17. MILNOR, W. R. Arterial impedance as ventricular afterload. *Circ. Res.* 36: 565–570, 1975.
18. MILNOR, W. R. *Hemodynamics.* Baltimore, MD: Williams & Wilkins, 1982, p. 312–337.
19. MILNOR, W. R., D. H. BERGEL, AND J. D. BARGAINER. Hydraulic power associated with pulmonary blood flow and its relation to heart rate. *Circ. Res.* 19: 467–480, 1966.
20. NYHAN, D. P., H. M. GOLL, B. B. CHEN, D. M. FEHR, P. W. CLOUGHERTY, AND P. A. MURRAY. Pentobarbital anesthesia alters pulmonary vascular response to neural antagonists. *Am. J. Physiol.* 256 (*Heart Circ. Physiol.* 25): H1384–H1392, 1989.
21. PANDIAN, N. G., A. WEINTRAUB, A. KREIS, S. L. SCHWARTZ, M. A. KONSTAM, AND D. N. SALEM. Intracardiac, intravascular high-frequency ultrasound imaging of pulmonary artery and its branches in humans and animals. *Circulation* 81: 2007–2012, 1990.
22. PATEL, D. J., AND D. L. FRY. In situ pressure-radius-length measurements in ascending aorta of anesthetized dogs. *J. Appl. Physiol.* 19: 413–416, 1964.
23. PATEL, D. J., D. P. SCHILDER, AND A. J. MALLOS. Mechanical properties and dimensions of the major pulmonary arteries. *J. Appl. Physiol.* 15: 92–96, 1960.
24. STEINER, R. E., S. FLICKER, W. J. ELDREDGE, R. M. MCMILLAN, H. NAIDECH, M. REES, AND R. S. ATLIN. The functional and anatomic evaluation of the cardiovascular system with rapid-acquisition computed tomography. *Radiol. Clin. North Am.* 24: 503–520, 1986.
25. WOMERSLEY, J. R. *The Mathematical Analysis of the Arterial Circulation in a State of Oscillatory Motion.* Wright Air Development Center, 1957. (Tech. Rep. WADC-TR56–614)